Molecular Therapy
Nucleic Acids
Original Article

miRNA-92a-3p regulates osteoblast differentiation in patients with concomitant limb fractures and TBI via IBSP/PI3K-AKT inhibition

Liangcong Hu,[1,4] Jing Liu,[1,4] Hang Xue,[1,4] Adriana C. Panayi,[2] Xudong Xie,[1] Ze Lin,[1] Tiantian Wang,[3] Yuan Xiong,[1] Yiqiang Hu,[1] Chengcheng Yan,[1] Lang Chen,[1] Abudula Abududilibaier,[1] Wu Zhou,[1] Bobin Mi,[1] and Guohui Liu[1]

[1]Department of Orthopedics, Union Hospital, Tongji Medical College, Huazhong University of Science and Technology, 1277 Jiefang Avenue, Wuhan 430022, China; [2]Division of Plastic Surgery, Brigham and Women's Hospital, Harvard Medical School, Boston 02215, USA; [3]Department of Emergency, Union Hospital, Tongji Medical College, Huazhong University of Science and Technology, 1277 Jiefang Avenue, Wuhan 430022, China

Patients who sustain concomitant fractures and traumatic brain injury (TBI) are known to have significantly quicker fracture-healing rates than patients with isolated fractures. The mechanisms underlying this phenomenon have yet to be identified. In the present study, we found that the upregulation of microRNA-92a-3p (miRNA-92a-3p) induced by TBI correlated with a decrease in integrin binding sialoprotein (IBSP) expression in callus formation. *In vitro*, overexpressing miRNA-92a-3p inhibited IBSP expression and accelerated osteoblast differentiation, whereas silencing of miRNA-92a-3p inhibited osteoblast activity. A decrease in IBSP facilitated osteoblast differentiation via the Phosphatidylinositol 3-kinase/threonine kinase 1 (PI3K/AKT) signaling pathway. Through luciferase assays, we found evidence that IBSP is a miRNA-92a-3p target gene that negatively regulates osteoblast differentiation. Moreover, the present study confirmed that pre-injection of agomiR-92a-3p leads to increased bone formation. Collectively, these results indicate that miRNA-92a-3p overexpression may be a key factor underlying the improved fracture healing observed in TBI patients. Upregulation of miRNA-92a-3p may therefore be a promising therapeutic strategy for promoting fracture healing and preventing nonunion.

INTRODUCTION

Ever since Calandriello's[1] seminal work in the 1960s that highlighted that patients with traumatic brain injury (TBI) and concomitant fractures display greater bone formation, numerous studies have established the critical role of TBI in bone-fracture healing. Patients with concomitant bone fractures and TBI have long been believed to heal more quickly than patients without TBI. A number of cross-sectional studies have suggested an association between TBI, rapid callus formation, and heterotopic ossification.[2,3] Surveys, such as that conducted by Brady et al.,[4] have shown that closed-head TBI results in calluses that are larger in size and with increased bone volume. Surprisingly, the underlying mechanisms of this phenomenon have not yet been closely examined.

Both bone remodeling and repair are involved in the process of fracture healing. Osteoblasts are the key cells for new bone formation during fracture healing.[5] It has previously been observed that osteoblast differentiation can be triggered by upregulating or downregulating the expression of cytokines, hormones, and growth factors.[6–8] It further affects the processes of mineralization, maturation, and proliferation of osteoblasts.[9–11]

MicroRNAs (miRNAs) are small, single-stranded, non-coding RNAs that widely exist in different tissues. They downregulate the expression of target genes mainly through mRNA degradation and transcription inhibition.[12,13] miRNAs have been demonstrated to be widely involved in the regulation of osteoblast differentiation and bone growth.[14–16] Most of these miRNAs have only been studied *in vitro*, and their pathophysiological mechanisms in patients with fracture and brain trauma, as well as in animal models, have not yet been fully established. The role of miRNAs on increasing bone callus healing in fractures and brain trauma and the study of the differentiation of osteogenic precursor cells is also unclear. After traumatic brain trauma, the expression of some miRNAs in the plasma and brain tissue of patients is expected to be abnormally increased. These miRNAs may participate in the repair process of injured brain tissue and limbs.[17,18]

Received 20 June 2020; accepted 8 February 2021;
https://doi.org/10.1016/j.omtn.2021.02.008.

[4]These authors contributed equally

Correspondence: Guohui Liu, Department of Orthopedics, Union Hospital, Tongji Medical College, Huazhong University of Science and Technology, 1277 Jiefang Avenue, Wuhan 430022, China.
E-mail: liuguohui@hust.edu.cn
Correspondence: Bobin Mi, Department of Orthopedics, Union Hospital, Tongji Medical College, Huazhong University of Science and Technology, 1277 Jiefang Avenue, Wuhan 430022, China.
E-mail: mibobin@hust.edu.cn
Correspondence: Wu Zhou, Department of Orthopedics, Union Hospital, Tongji Medical College, Huazhong University of Science and Technology, 1277 Jiefang Avenue, Wuhan 430022, China.
E-mail: 2016XH0120@hust.edu.cn

miRNA-92a-3p is a single-stranded, non-coding RNA that has been reported to participate in regulating angiogenesis, inhibiting apoptosis, enhancing chondrocyte production, and inhibiting cartilage degradation.[19,20] Redell et al.[18] reported that the expression level of miRNA-92a-3p increases significantly in the first 24 h after mild TBI injury but decreases in severe TBI patients. Thus far, little attention has been paid to the role of miRNA-92a-3p on the differentiation of osteogenic precursor cells into osteoblasts, especially in situations of concomitant fracture and traumatic brain trauma.

The gene integrin binding sialoprotein (IBSP), which is located on chromosome 4q28-q31, is composed of six small exons (51 to 159 bp) and one large exon (~2.6 kb).[21] The physiological role of IBSP in the population is mainly to encode the main structural protein of bone matrix, which constitutes approximately 12% of non-collagen protein in human bone tissue and is synthesized by bone-related cells such as osteoblasts, bone cells, and osteoclasts.[22–24] The PI3K/AKT signaling pathway is widely involved in bone repair and bone development, and plays an important role in controlling bone cell number and mass, as well as new bone formation.[25,26] The exact physiological role of IBSP, as well as the miRNAs that serve as its upstream regulators, has yet to be verified.

This study attempts to elucidate the potential molecular mechanism that underlies the increase in formation of callus and speed of fracture healing in patients with concomitant fractures and traumatic brain injury. We focus our investigation on the rapid increase in miRNA-92a-3p expression levels that have been noted to occur within 24 h after moderate traumatic brain injury. In addition, direct targeted IBSP is used to detect the effects of miRNA-92a-3p and its antagonists (antagomiRNA-92a-3p) on the differentiation and maturation of osteoblast precursor cells to osteoblasts.

RESULTS

miRNA-92a-3p expression is elevated in the plasma and callus of clinical patients with fracture and brain trauma

Previous studies have shown that fracture healing in patients with concomitant fractures and brain trauma is faster than that of isolated fractures.[27] In TBI patients, expression of miRNA-92a-3p in injured brain tissue and peripheral blood is upregulated.[17,18] miRNA-92a participates in the differentiation of osteoblast precursor cells into osteoblasts and can promote chondrogenesis.[19,28] In order to investigate the fracture healing and miRNA-92a-3p expression in patients with concomitant fractures and brain trauma, we collected samples from 30 patients (10 cases with completely healed fractures, 10 cases with isolated fractures, and 10 cases with concomitant fractures and brain trauma). The expression levels of miRNA-92a-3p in the plasma and callus were detected using RT-PCR. The healing of the two groups of patients (isolated fractures, and concomitant fractures and brain trauma) of the same fracture type and at the same follow-up time was evaluated using X-rays. In order to minimize the influence of gender, age, and different degrees of brain trauma on the expression of miRNA-92a-3p and fracture healing, we set strict inclusion criteria: female, aged 25–40 years, closed fracture, mild to moderate brain trauma with concomitant fracture (Glasgow Coma Scale [GCS] score 8–14 points), and no prior history of diabetes, hypertension, heart disease, and cerebrovascular disease. The results showed that in the same site and type of fracture, the fracture healing time of the group with concomitant brain trauma and fracture was shorter than that of the isolated fracture group (Figures 1A and 1B; Figure S1). RT-PCR results showed that the level of plasma miRNA-92a-3p expression in the concomitant fracture and brain trauma group was significantly higher than that of the other two groups on the 1st day, the 3rd day, and the 7th day after admission (Figure 1C). The expression level of miRNA-92a-3p in the bone callus of the isolated fracture group was significantly lower than that of the concomitant fracture and brain trauma group (Figure 1D); on the 14th day after injury, the new bone callus in the concomitant fracture and brain trauma group was more pronounced than that of the isolated fracture (Figures 1E and 1F; Figure S2).

Plasma and callus miRNA-92a-3p expression is upregulated in the fracture and TBI mouse model

In order to further verify the experimental results of clinical observation, we used female, 8-week-old C57BL/6J mice to induce femoral fracture and brain injury models. On the 3rd, 7th, and 14th days after modeling, the expression levels of miRNA-92a-3p in peripheral blood of mice were detected using RT-PCR. On the 14th and 21st days after surgery, quantitative micro-computed tomography (mCT) was used to scan the fractured femur of mice, and the key indicators of bone formation and three-dimensional reconstruction images were analyzed. The results showed that the expression level of miRNA-92a-3p in the peripheral blood of the group with concomitant fracture and brain trauma was higher than that of the isolated fracture group and of the control group (Figure 2A). mCT scan results showed that the bones of the group with concomitant fracture and brain trauma had significantly higher scab volumes, bone volume (BV), tissue volume (TV), bone mass density (BMD), and percent bone volume (BV/TV) than the isolated fracture group (Figures 2B–2F).

miRNA-92a-3p promotes osteoblastogenesis and matrix mineralization

To evaluate the effect of miRNA-92a-3p on matrix mineralization and osteoblastogenesis, we used lipo3000 to transfect agomiR92a-3p, antagomiR-92a-3p, agomiR-negative control (NC), antagomiR-NC, or PBS (control group) into MC3T3-E1 subclone 14 cells. 48 h after transfection, RT-PCR was used to detect the transfection effect and osteogenic gene expression, and western blotting was used to detect the expression of the osteogenic marker protein. On day 14 and day 21 after transfection, alkaline phosphatase and alizarin red staining were used to detect the mineralization of extracellular matrix. RT-PCR results showed that the expression of miRNA-92a-3p was upregulated in the agomiR-92a-3p group (Figure 3A). The expression levels of the osteogenic genes bone gamma-carboxyglutamate protein (OCN), RUNX2, alkaline phosphatase staining (ALP), and Col1a1 in the agomiR-92a-3p treatment group were significantly higher than that of the antagomiR- 92a-3p group (Figures 3B–3E); western

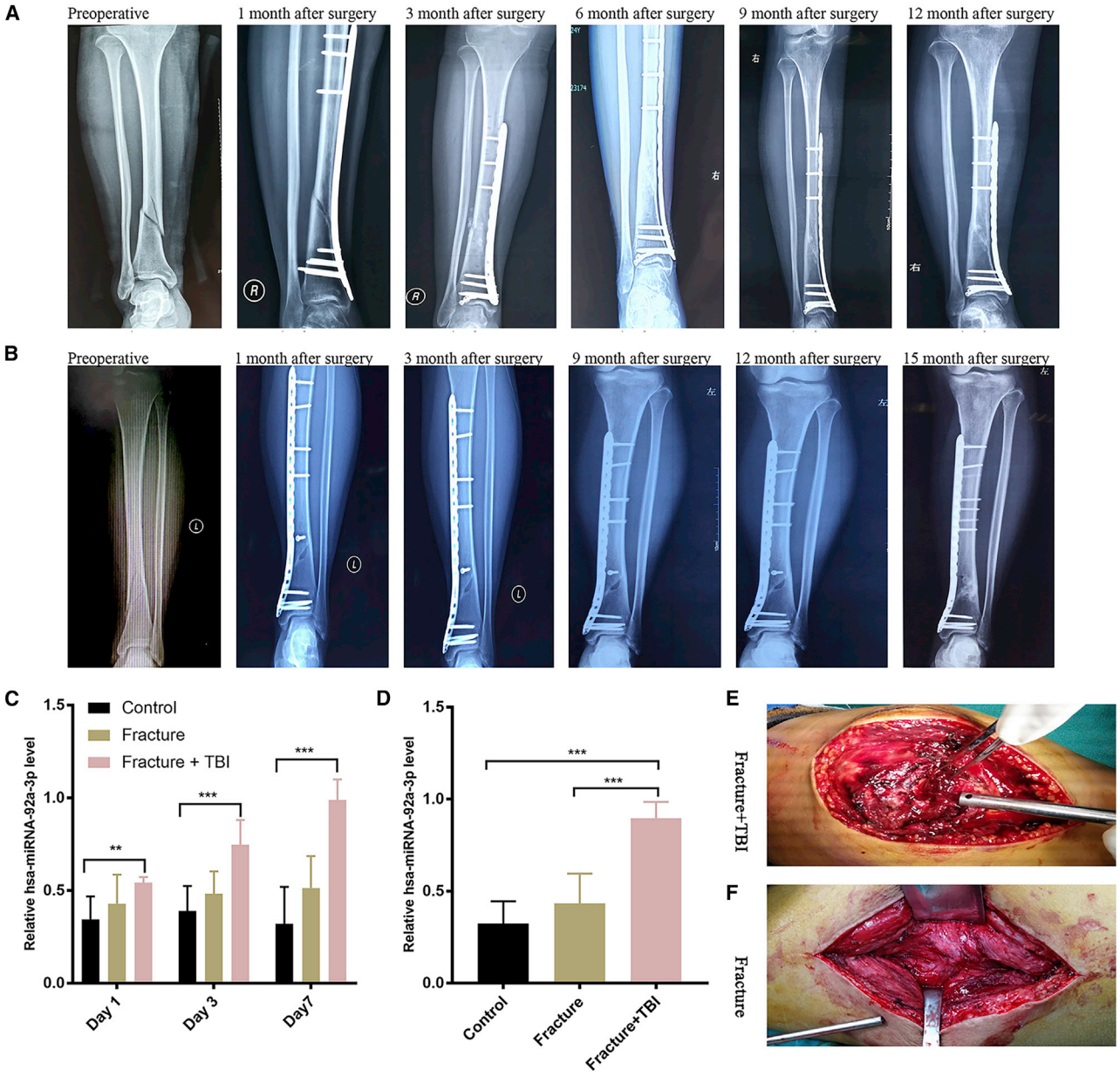

Figure 1. miRNA-92a-3p expression is elevated in the plasma and callus of patients with concomitant extremity fractures and brain trauma

(A) 34-year-old female patient with concomitant fracture of the distal tibia and brain trauma. X-rays of the anterior and posterior tibia and fibula at 1 week before surgery, and 1 month, 3 months, 6 months, 9 months, and 12 months after surgery. (B) 32-year-old female patient with fracture of the distal tibia. X-rays of the anterior and posterior tibia and fibula at 1 week before surgery, and at 1 month, 3 months, 6 months, 9 months, and 15 months after surgery. (C) miRNA-92a-3p plasma expression. RT-PCR showed that the level of miRNA-92a-3p expression in the plasma of the concomitant fracture and traumatic brain injury (TBI) group was significantly higher than that of the other two groups on day 1, day 3, and day 7 since admission. (D) miRNA-92a-3p callus expression. RT-PCR results showed that the expression level of miRNA-92a-3p in the callus of the concomitant fracture and TBI group was significantly higher than that of the other two groups. (E and F) In the second week after injury, patients with concomitant fracture and TBI were more susceptible to callus formation than those with isolated fractures. N = 10; data are presented as mean ± SD (*$p < 0.05$; **$p < 0.01$; ***$p < 0.001$; # no significance).

blotting showed that the expression levels of the bone-formation marker proteins OCN, RUNX2, ALP, and Col1a1 in the agomiR-92a-3p treatment group were significantly higher than those in the antagomiR-92a-3p group (Figure 3F). Alkaline phosphatase staining on day 14 showed that mineralization of extracellular matrix in the agomiR-92a-3p treatment group was significantly higher than that

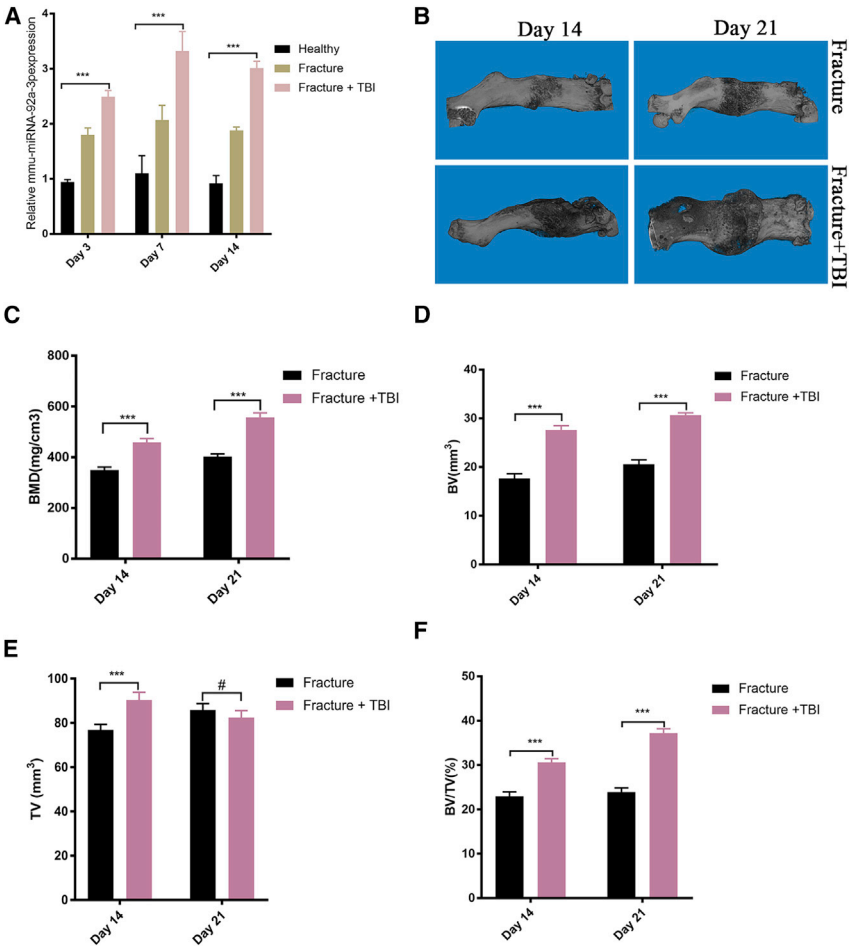

Figure 2. miRNA-92a-3p expression is upregulated in the plasma and callus of the fracture + TBI mouse model

(A) miRNA-92a-3p plasma expression. RT-PCR showed that on day 3, day 7, and day 14 after modeling, the relative expression level of plasma miRNA-92a-3p in the femoral Fracture+TBI group was significantly higher than that in other groups. (B) Micro-CT (mCT) scan reconstruction of femoral callus. On day 14 and day 21 after modeling, the callus in the Fracture+TBI group was more evident than that in the isolated Fracture group. (C–F) mCT measurements of femoral callus at day 14 and day 21 after fracture modeling. Bone mass density (BMD), tissue volume (TV), bone volume (BV), and percent bone volume (BV/TV) are displayed. n = 5; data are presented as mean ± SD (*p < 0.05; **p < 0.01; ***p < 0.001; # no significance).

in the antagomiR-92a-3p group (Figure 3G; Figure S3). This was verified with alizarin red staining on day 21 (Figure 3H; Figure S4).

miRNA-92a-3p directly targets IBSP

To investigate whether miRNA-92a-3p directly targets IBSP, we used four online miRNA target gene prediction sites and used the online Venn diagram (http://bioinformatics.psb.ugent.be/webtools/Venn/) to predict the target genes of the four sites (mirDB, mirwalk, TargetScan, and miRanda). Identifying the intersection, we found that miRNA-92a-3p directly targets IBSP (Figure 4A). In order to further verify the direct targeting of miRNA-92a-3p, we used either a wild-type (WT) IBSP 3′ UTR or a mutant-type (Mut) IBSP 3′ UTR construct fused to a luciferase reporter (Figure 4B). Using these constructs, the results showed that silent miRNA-92a-3p (antagomiR-92a-3p group) can significantly increase the WT IBSP 3′ UTR reporter activity (Figure 4B), but not the Mut IBSP 3′ UTR reporter activity (Figure 4C). When transfecting MC3T3E1 cells with antagomiR-92a-3p to reduce endogenous miRNA-92a-3p expression level, WT IBSP 3′ UTR reporter activity increased significantly (Figures 4B and 4C). After 48 h, RT-PCR was used to detect the IBSP mRNA expression level, and western blotting was used to detect the IBSP protein expression level. The results showed that overexpression of miRNA-92a-3p (agomiR-92a-3p group) can significantly reduce the expression of IBSP protein and genes in MC3T3-E1 subclone 14 cells (Figures 4D and 4E). In order to further study the correlation between miRNA-92a-3p and IBSP in concomitant fracture and brain trauma, we investigated the expression of IBSP in both human patients and murine models. Western blotting and IHC were used to detect the IBSP level of callus of patients and mice in different groups. The results showed that the expression level of IBSP in the group with concomitant fracture and brain trauma was significantly lower than that in other groups (Figures 4F–4H). To investigate whether the differentiation of osteogenic precursor cells into osteoblasts is dependent on IBSP, we used the interfering RNA construct in IBSP to transfect bone precursor cells. After 48 h, western blotting and RT-PCR were used to detect the expression of key osteogenic target genes and proteins. The results showed that the key marker proteins and genes of osteogenesis in the small interfering IBSP (si-IBSP) treatment group were significantly higher than those in the control group and siRNA-NC group (Figures 4I and 4J). In summary, our experimental results confirm that miRNA-92a-3p directly targets the 3′ UTR of IBSP to differentiate osteogenic precursor cells into osteoblasts.

PI3K/AKT signaling is involved in IBSP-regulated osteoblast differentiation

In order to further explain the relationship between IBSP and the PI3K/AKT signaling pathway, we transfected MC3T3-E1 subclone 14 cells with different miRNAs. After 48 h, western blotting was used to detect the protein-expression levels of AKT, p-AKT, PI3K, and p-PI3K. The results showed that overexpression of miRNA-92a-3p (agomiRNA-92a-3p) can significantly increase the protein expression levels of p-AKT and p-PI3K (Figure 5A). In order to investigate how the PI3K/AKT signaling pathway is affected by IBSP, we used

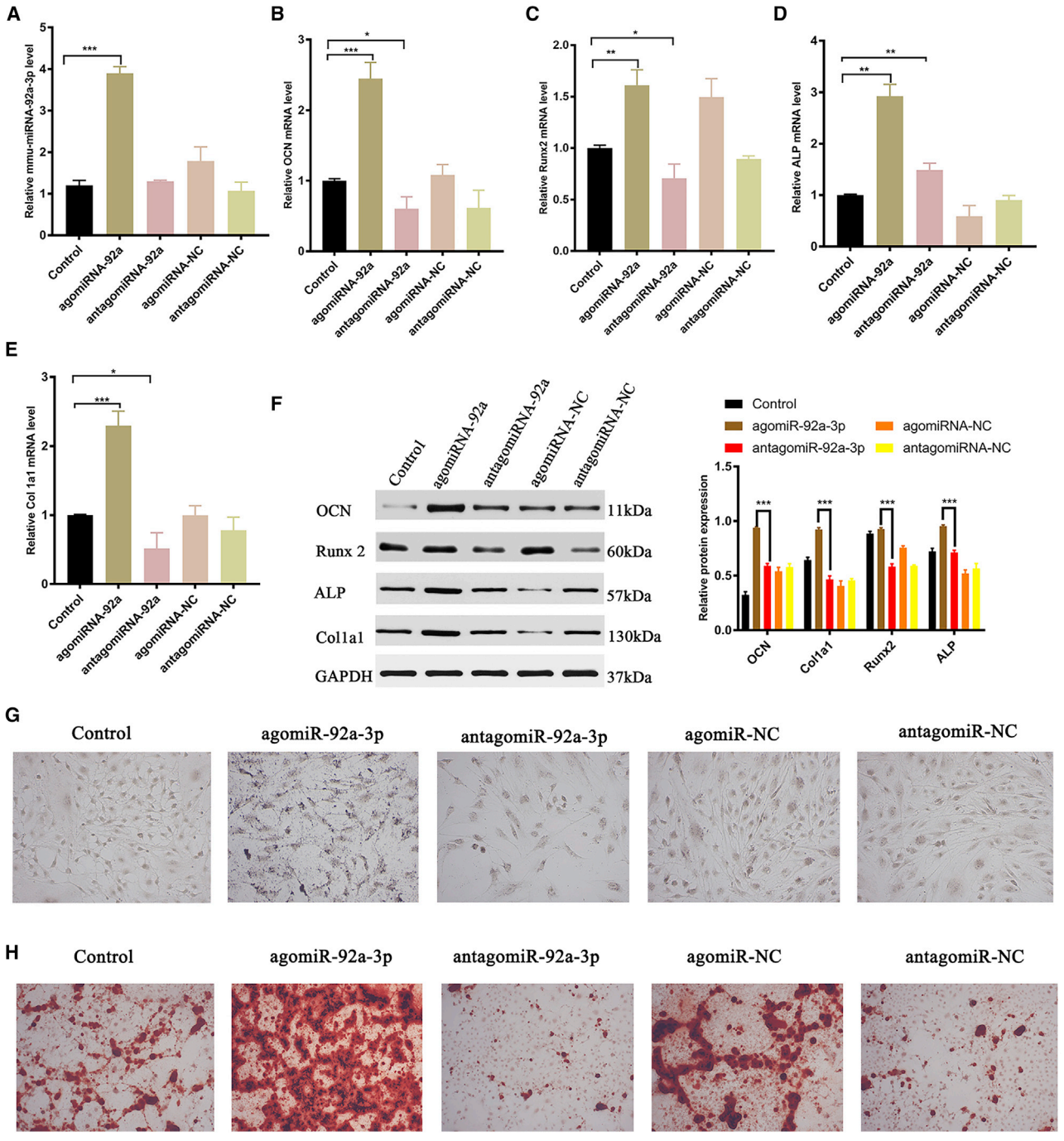

Figure 3. miRNA-92a-3p promotes osteoblastogenesis and matrix mineralization

Transfection of agomiRNA-92a-3p, antagomiRNA-92a-3p, agomiRNA-NC, antagomiRNA-NC, and Lipofectamine 3000 control (200 μm) in MC3T3-E1 cells for 48 h. (A) RT-PCR showed that mmu-miRNA-92a-3p expression was upregulated in agomiRNA-92a-3p. (B) RT-PCR showed that OCN expression was upregulated in agomiRNA-92a-3p. (C) RT-PCR showed that Runx2 expression was upregulated in agomiRNA-92a-3p. (D) RT-PCR showed that Alkaline phosphatase staining (ALP) expression was upregulated in agomiRNA-92a-3p. (E) RT-PCR showed that mRNA expression was upregulated in agomiRNA-92a-3p. (F) Western blotting to evaluate the expression of OCN, Runx2, ALP, and Col1a1 protein after 48 h. (G) ALP after 14 days (scale bar, 10 mm). (H) Alizarin red-mediated calcium staining after 21 days. n = 3; data are presented as mean ± SD (*$p < 0.05$; **$p < 0.01$; ***$p < 0.001$; # no significance).

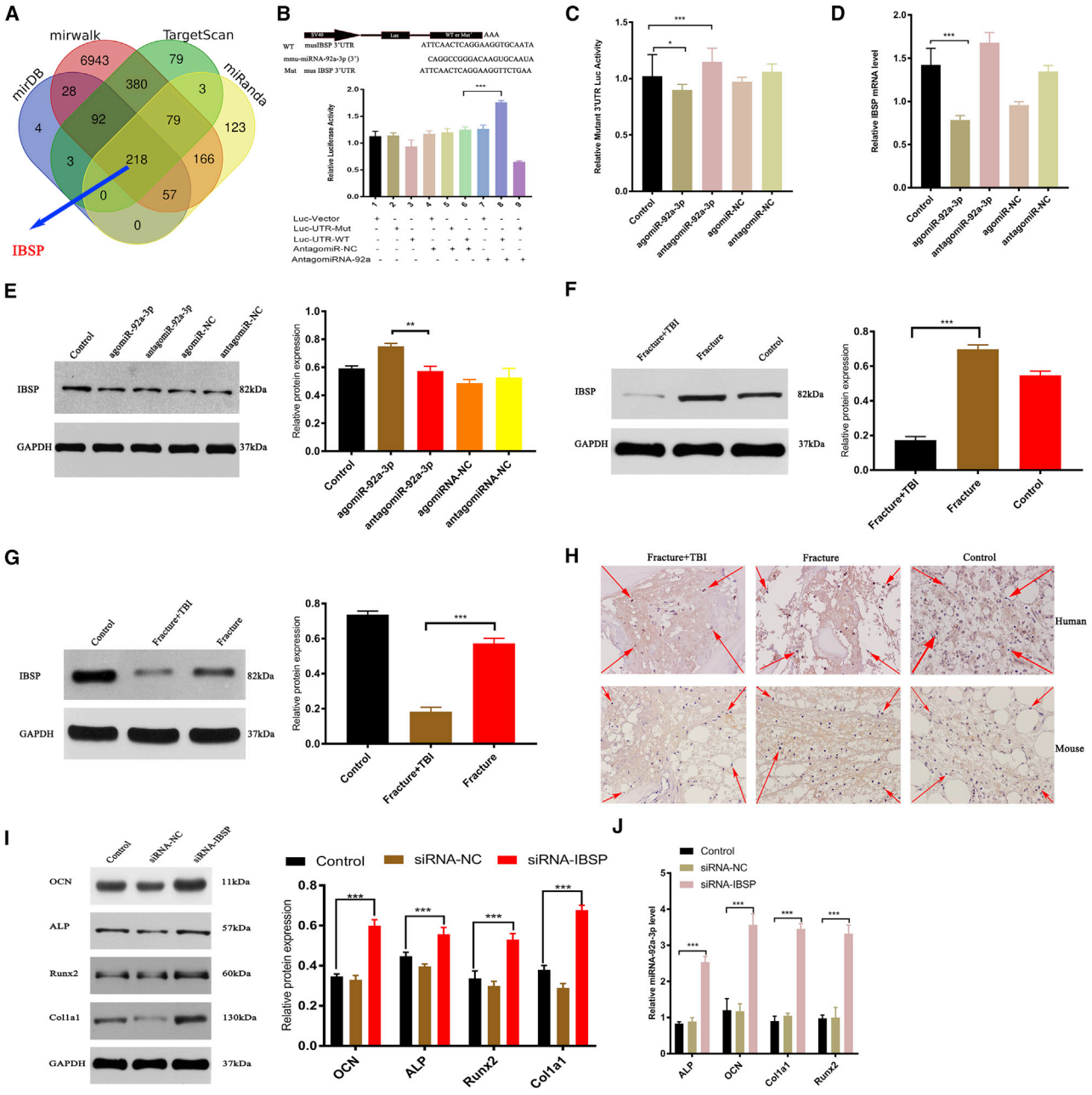

Figure 4. miRNA-92a-3p directly targets IBSP

(A) Prediction of the miRNA-92a-3p target gene. Using four online miRNA target gene prediction sites and visualizing the intersection of the Venn diagrams identifies ISBP as a target gene at all four sites. (B) The predicted luciferase (Luc) reporter gene construct contains WT IBSP 3′ UTR (WT 3′ UTR) or the same region after site-directed mutagenesis (3′ UTR-Mut). (C) Luciferase activity after treatment with antagomiR-92a-3p to investigate the effect of endogenous miRNA-92a-3p in MC3T3-E1 cells on IBSP 3′ UTR Muts (WT IBSP 3′ UTR, lucu-UTR-mut). (D and E) After transfection of the control group, agomiR-92a-3p, agomiR-NC, antagomiR-92a-3p, and antagomiR-NC, (D) qPCR, and (E) western blot analyses were used to detect the expression of IBSP. (F) Expression of IBSP in the control group, Fracture group, Fracture+TBI group. (G) Expression of IBSP in bone callus tissue of Fracture and Fracture+TBI mice. (H) Immunohistochemistry showed decreased expression of IBSP protein in the Fracture+TBI callus (the red arrow shows the positive IBSP immunohistochemical staining). (I and J) Transfection of MC3T3-E1 subclone 14 cells with siRNA (control), siRNA-NC, and siRNA-IBSP, and subsequent evaluation of Col1a1, ALP, OCN, and Runx2 using (I) western blot and (J) RT-PCR analysis. n = 3; data are presented as mean ± SD (*$p < 0.05$; **$p < 0.01$; ***$p < 0.001$; # no significance).

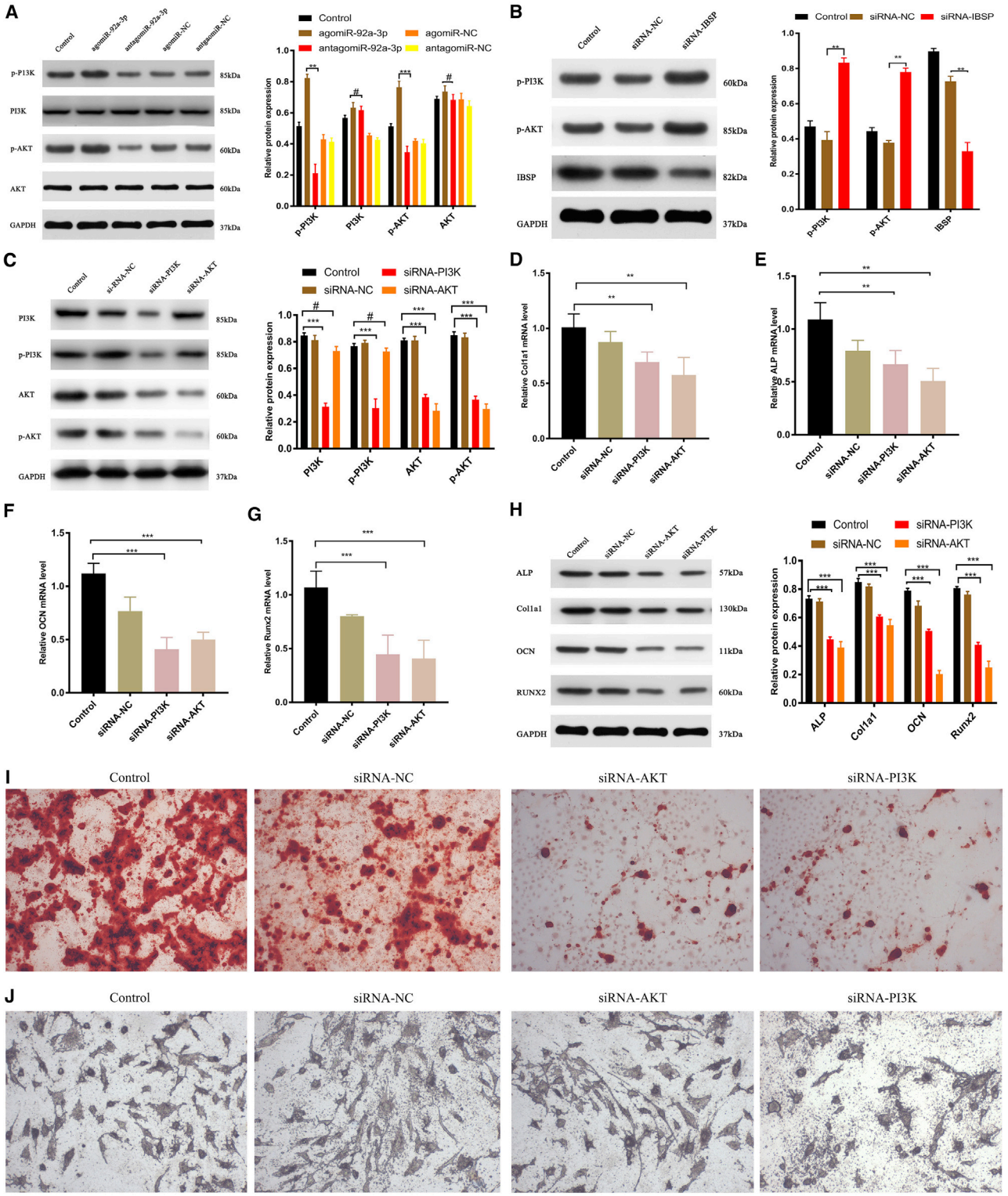

Figure 5. PI3K/AKT signaling is involved in IBSP-regulated osteoblast differentiation

(A) Transfection of agomiRNA-92a-3p, antagomiRNA-92a-3p, agomiRNA-NC, antagomiRNA-NC, and Lipofectamine 3000 control (200 μm) in MC3T3-E1 cells for 48 h. Western blot detection of the expression of PI3K and AKT after transfection. (B) Western blot detection of IBSP, p-PI3K, and p-AKT levels after transfection with siRNA-NC,

(legend continued on next page)

IBSP-interfering RNA (si-IBSP), PI3K siRNA, and AKT siRNA to transfect MC3T3-E1 subclone 14 cells and used western blotting to investigate their role in the PI3K/AKT signaling pathway 48 h later. The results showed that IBSP siRNA can significantly increase the phosphorylation levels of PI3K and AKT and significantly inhibit IBSP protein expression (Figure 5B). PI3K siRNA can significantly inhibit the phosphorylation levels of PI3K and AKT and the PI3K and AKT protein expression. AKT siRNA can significantly inhibit the phosphorylation levels of AKT and AKT protein expression (Figure 5C).

In order to explore the effect of the PI3K/AKT signaling pathway on the osteogenic and extracellular matrix mineralization ability of the osteogenic precursor cells, we used PI3K siRNA and AKT siRNA to transfect MC3T3-E1 subclone 14 cells. After 48 h, western blotting and RT-PCR were used to detect the target protein and gene of the osteogenic markers, respectively. We found that use of si-PI3K and si-AKT inhibited PI3K and AKT, and the expression levels of osteogenesis target protein and target gene were significantly lower than that of the control group (Figures 5C–5H). Alkaline phosphatase and alizarin red staining were performed on day 14 and day 21 after transfection to detect the osteogenic differentiation and extracellular matrix mineral deposition of MC3T3-E1 subclone 14 cells. The results showed that MC3T3-E1 subclone 14 cells treated with si-PI3K and si-AKT had decreased extracellular matrix mineralization (Figures 5I and 5J; Figures S5 and S6).

Local administration of miRNA-92a-3p accelerates femur fracture healing in mice

To verify the osteogenic ability of miRNA-92a-3p *in vivo*, we utilized a previously described method.[29] Briefly, on the 1st, 3rd, and 7th day after fracture model-establishment, mice were injected with agomiRNA-92a-3p, antagomiRNA-92a-3p, PBS. On the 21st day after surgery, mCT scan analysis was performed to evaluate the callus formation volume and establish the bone-formation parameters. H&E staining was used to evaluate local bone remodeling. RT-PCR was used to evaluate the expression of bone callus marker gene. The results showed that bone callus volume (Figures 6A–6C) and the bone-formation parameters of the agomiRNA-92a-3p injection group were significantly higher than other groups (Figures 6G–6J). H&E staining highlighted that the trabecular bones in the agomiR-92a-3p group were denser and the fracture healing effect was more obvious than other groups (Figures 6D–6F). The expression level of osteogenic target genes in the callus area in the agomiR-92a-3p group was significantly higher than in other groups on RT-PCR on day 21 (Figures 6K–6N). Western blotting to detect the expression of osteogenic marker protein in the callus on day 14 and day 21 showed that the expression level of the osteogenic marker protein on the callus on day 14 and day 21 of the agomiR-92a-3p group was significantly higher than in other groups (Figures 6O and 6P). These results confirm that miRNA-92a-3p plays a positive regulatory role in fracture healing.

DISCUSSION

As traffic injury occurrence continues to increase, injuries with concomitant traumatic fractures and brain trauma have become more prevalent.[30–33] Despite the continuous optimization and innovation of surgical techniques and instruments, success of fracture healing is still not fully guaranteed. Fracture nonunion and delayed healing are difficulties faced by many trauma and orthopedic surgeons, irrespective of experience and expertise.[34,35] Current strategies for treating fracture nonunion require reoperation, which is disadvantageous for the patient, both in terms of health and recovery, as well as economically, as it incurs a high economic burden. Even after secondary surgery, the success rate of fracture healing cannot be guaranteed.[36,37] Therefore, it is urgent to carry out more effective and convenient for fracture nonunion treatment.

Prior studies have noted that patients with concomitant fractures and brain trauma display faster callus formation and more efficient fracture healing than simple fractures.[4,38,39] Therefore, concomitant TBI may affect the expression of osteogenic genes and the balance of bone remodeling through certain direct or indirect factors, resulting in accelerated callus formation and fracture healing. According to previous studies, within 24 h after TBI injury abnormal expression of multiple miRNAs in plasma can be seen.[17,18,40] In agreement with our current results, previous studies have demonstrated that a variety of miRNAs at the post-transcription level negatively regulate gene expression by binding to the targeted mRNA and participate in the regulation of the bone remodeling process.[41,42] Currently, research on the increased fracture healing and bone callus formation seen in concomitant brain trauma has largely focused on investigating the effect of cytokines and other proteins, while research on the regulation of miRNAs is still lacking.[43–45] However, our study found that the expression level of miRNAs-92a-3p was significantly increased in patients with concomitant fractures and brain trauma, as well as in the mouse model. miRNAs-92a-3p can promote the mineralization and maturation of osteoblast precursor cells *in vitro*, and local injection of agomiR-92a-3p can significantly promote scab formation at the fracture site in mice. This finding of our study indicated that miRNA-92a-3p can promote the maturation and mineralization of osteoblast precursor cells *in vitro*, thereby accelerating the healing rate of fractures in patients with concomitant fractures and brain trauma.

Prior studies have noted that miRNA-92a-3p is expressed in peripheral blood, exosomes of colon cancer patients, chondrocytes, and bone marrow mesenchymal stem cells. Biological functions of

siRNA-IBSP, and controls for 48 h. (C–G) Transfection with Lipofectamine 3000, siRNA-NC, siRNA-PI3K, or siRNA-AKT for 48 h. (C) Protein-expression levels of p-AKT, AKT, p-PI3K, and p-PI3K using western blotting. (D–G) qPCR analysis of Col1a1 (D), ALP (E), OCN (F), and Runx2 (G) expression in bone precursor cells. (H) Western blot analysis of Col1a1, ALP, OCN, and Runx2 levels 48 h after transfection. (I) Alizarin red staining of MC3T3-E1 cells 3 weeks after transfection. (J) ALP staining of MC3T3-E1 cells 2 weeks after transfection. n = 3; data are presented as mean ± SD (*$p < 0.05$; **$p < 0.01$; ***$p < 0.001$; # no significance).

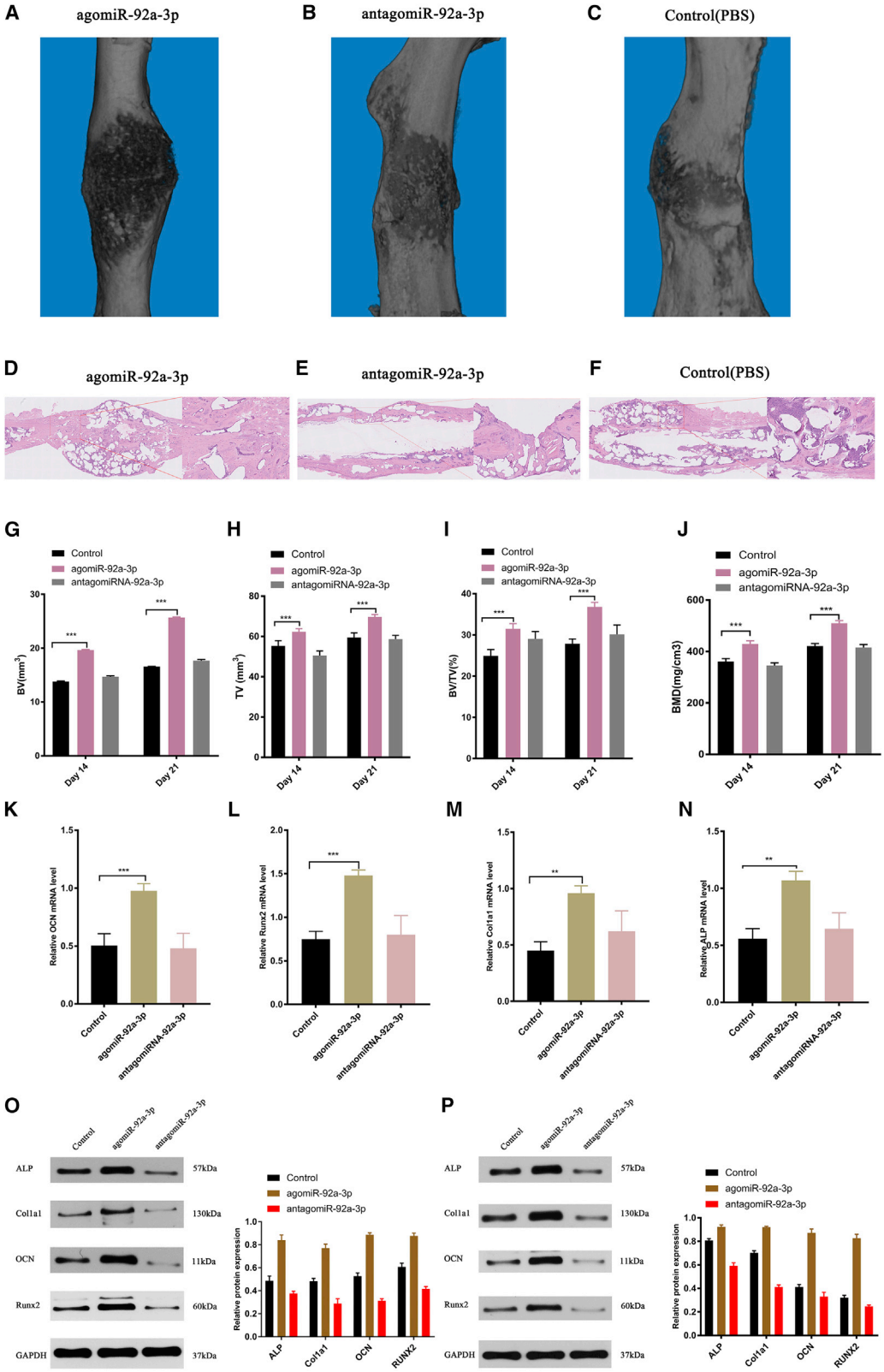

(legend on next page)

miRNA-92a-3p that have been identified include inhibition of spinal cord cell apoptosis, enhancement of chondrogenesis, suppression of cartilage degradation, promotion of myogenic-lineage differentiation, and attenuation of cardiac apoptosis. Therefore, miRNA-92a-3p appears to be involved in the regulation of cell maturation, differentiation, apoptosis, and immune regulation.[19,20,46,47] Redell et al.[17,18] reported that miRNA-92a-3p expression was upregulated 24 h after injury in TBI patients, a conclusion that agrees with both the clinical and animal model results of our current study. We further elucidated the role of miRNA-92a-3p in fracture healing, by suggesting a novel possible mechanism through which miRNA-92a-3p regulates the expression of IBSP in bone tissue and osteogenic precursor cells. When the expression of IBSP was suppressed, it led to the upregulation of osteogenesis-related gene expression and promoted bone formation. The experimental results showed that changes in the level of miRNA-92a-3p regulated the expression of IBSP, suggesting that IBSP may be a functional target gene of miRNA-92a-3p, thus confirming that miRNA-92a-3p indeed has the ability to regulate bone formation. The osteoponin protein (IBSP), also known as osteoponin, is highly expressed in osteoblasts, osteoclasts, and hypertrophic chondrocytes. IBSP expression in the initial stage is mainly localized at the original bone-formation site, coupled with the initial membrane and endochondral bone-formation process, and IBSP expression level reaches its peak during embryonic bone formation. Knockout of IBSP in adult mice showed decreased number and surface area of osteoclasts, and the recruitment and activity of osteoclasts *in vivo* is unbalanced in the absence of IBSP.[48,49] According to literature search results, inhibition or knockdown of IBSP can inhibit the number, function, and activity of osteoclasts. Our experimental results showed that overexpression of miR-92A-3p can inhibit the expression of IBSP and promote the expression of osteoblast-related proteins. These results strongly suggest that osteoclast activity is inhibited or decreased during this process.

The PI3K/AKT signaling pathway is widely involved in the phenotypic regulation of multiple different cells and diseases.[50,51] Prior research has shown that the PI3K/AKT signaling pathway is involved in the bone metabolism and remodeling process.[52,53] Liu et al.[54] and others showed that the PI3K/AKT signaling pathway is involved in regulating osteogenic precursor cell differentiation and activity.[55] Furthermore, various studies have supported that the PI3K/AKT signaling pathway may be involved in regulating the progress of osteoporosis through IBSP.[26,52] In this study, we identified that downregulation of IBSP expression can activate the PI3K/AKT signaling pathway, leading to increased transcriptional expression of osteoblast-specific target genes.

In this study, miRNA-92a-3p expression analysis was performed on plasma from adult female patients with fractures and concomitant moderate head trauma. The exclusion criteria were strict so as to minimize any expression differences caused by variations in the age, gender, or degree of brain trauma of the patients. In future experiments, we hope to investigate the expression level of miRNAs in patients with different ages, genders, and degrees of brain trauma. In addition, due to limitations and variations in clinical practice, we were not able to obtain a callus from all patients at the exact same time post-injury. Therefore, this may result in variations in the expression level of miRNA-92a-3p in the callus. In addition, bone cells, osteoclasts, vascular endothelial cells, and other cells are also involved in the process of bone reconstruction. However, in this research, we only verified expression in osteogenic precursor cells. Whether miRNA-92a-3p has an effect on other cells to promote osteogenesis is unclear and requires further research.

Conclusions

Our results identify that overexpression of miRNA-92a-3p *in vitro* can promote the differentiation of MC3T3-E1 cells into osteoblasts and provide evidence, for the first time, that the PI3K/AKT signaling pathway may be involved. In addition, we show that overexpression of miRNA-92a-3p can inhibit the expression of IBSP, and this silencing of IBSP leads to increased phosphorylation levels of PI3K and AKT and upregulation of the expression of key genes in osteogenesis(Figure 7). It is suggested that overexpression of miRNA-92a-3p promotes bone formation at the fracture site. Overall, we can conclude that fractures concomitant with brain trauma increase the expression level of miRNA-92a-3p in the circulation, which in turn inhibits the expression of IBSP at the fracture site, activating the PI3K/AKT signaling pathway and promoting the translation and transcription of osteogenic genes, hence accelerating fracture healing and callus formation. Therefore, induction of overexpression of miRNA-92a-3p at the fracture site may be a promising treatment for promoting fracture healing.

MATERIALS AND METHODS

Human plasma and bone tissue preparation

Serum from 30 female patients (10 completely healed fracture patients, 10 concomitant fracture and TBI patients, and 10 isolated fracture patients) was obtained from the Union Hospital, Tongji Medical College, Huazhong University of Science and Technology, via venous blood draw. 15 calluses were obtained from the patients who had fractures or concomitant fracture and TBI. The details of these patients are shown in Table 1. The average age of the completely healed fracture group was 34.2 ± 2.56 years, of the isolated fracture group was

Figure 6. Local administration of miRNA-92a-3p accelerates femur fracture healing in mice

(A–C) mCT-produced 3D images of bone callus formation at the fracture site on day 21 after modeling, comparing the (A) agomiRNA-92a-3p group, (B) antagomiRNA-92a-3p group, and (C) control group healing (PBS). (D–F) H&E tissue section staining comparing the (D) agomiRNA-92a-3p group, I antagomiRNA-92a-3p group, and (F) control group fracture-end healing on day 21 after modeling. (G–J) Analysis of the mCT presenting the BV (G), TV (H), BV/TV (I), and BMD (J) of bone callus on day 21 after modeling. (K–N) qPCR analysis of Col1a1 (M), ALP (N), OCN (K), and Runx2 (L) expression in the control, agomiR-92a-3p, antagomirmiR-92a-3p group on day 21 after modeling. (O and P) Western blot analysis of Col1a1, ALP, OCN, and Runx2 levels in the control, agomiR-92a-3p, and antagomiR-92a-3p group on day 14 (O) and day 21 (P) after modeling. n = 5; data are presented as mean ± SD (*p < 0.05; **p < 0.01; ***p < 0.001; # no significance).

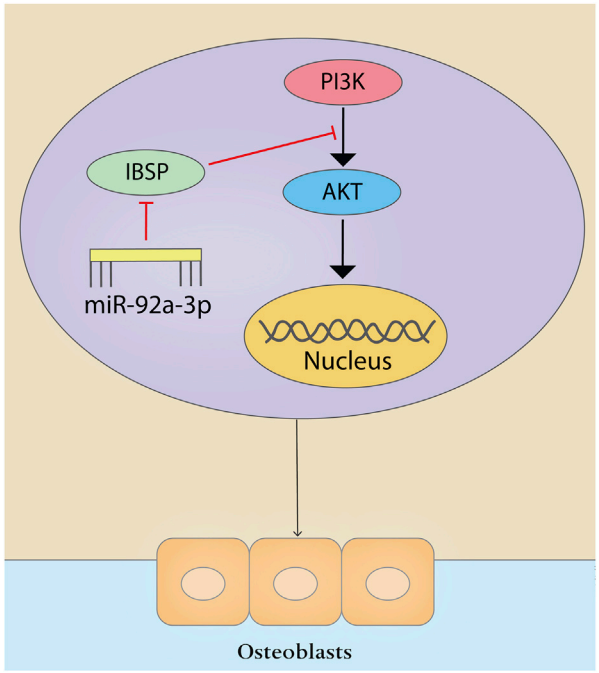

Figure 7. miRNA-92a-3p-mediated osteoblast differentiation
Schematic representation of the mechanism through which miRNA-92a-3p mediates the differentiation of osteogenic precursor cells into osteoblasts.

32.6 ± 3.35 years, and of the concomitant fracture and TBI group was 33.3 ± 2.93 years. All patients underwent X-ray examination of the fracture site after admission, and refer to the quantitative calculation method of callus proposed by Perkins et al.[56] If the fracture was near the joint, CT examination was also performed. If any ligament, nerve, and other soft tissue injuries were suspected, MRI examination was added to confirm the diagnosis. After admission, patients in the concomitant fracture and TBI group first underwent CT scanning of the brain, and their brain injury was graded according to the GCS (full score is 15 points, mild is 13–14 points, moderate is 9–12 points, and severe is 3–8 points). In the present study, we analyzed the peripheral blood in female patients to eliminate the potential differing effects of gender. All patients included had mild or moderate brain trauma.[57] All patients with concomitant fracture and TBI had moderate brain injury. Admitted participants were excluded if they were male, younger than 25 years old, older than 40 years old, and had prior significant medical history such as cerebrovascular disease, cardiovascular disease, diabetes, hypertension, COPD, and open fracture. This experiment was approved by the Medical Ethics Management Department of Tongji Medical College of Huazhong University of Science and Technology (ethics approval number: [2018] S431). Subjects provided fully informed consent.

Animal selection

A total of 30 female C57BL/6J mice aged 8 weeks was obtained from The Center of Experimental Animals, Tongji Medical College, Huazhong University of Science and Technology. The Institutional Animal Care and Use Committee at Tongji Medical College, Huazhong University of Science and Technology, approved all animal studies.

Mouse femoral fracture model

30 mice were anesthetized with 1% pentobarbital sodium (0.1 mL/10 g body weight) through intraperitoneal injection. The mice were placed on the left side, and the full length of the right thigh was prepared by removing the hair and disinfecting. A 1.0 cm incision was made on the right lateral thigh of the mouse along the longitudinal axis of the femur, and the muscles of the lateral thigh were exposed layer by layer from the proximal femur to the distal femur. The quadriceps femoris was longitudinally cut and a sharp knife was used to expose the distal femur. A 23-gauge intramedullary nail was inserted on to the femur longitudinally along the horizontal of the medullary cavity, and a fracture was created by trephine cutting the middle part of the femur with ophthalmic scissors.[58] 5 of these mice were then set aside as reserve and 25 mice were randomly divided into 5 groups, with 5 mice per group: normal, agomiR-92a-3p, antagomir-92a-3, Fracture, and Fracture+TBI. Local injection of miRNA was performed on days 1, 3, and 7 after modeling, with a single dose of 20 μmol/L in 100 μL PBS. 14 and 21 days after modeling, the mice were sacrificed by intraperitoneal injection of excessive pentobarbital sodium. The femoral bone on the modeling side was harvested, the soft tissues and muscles were removed, and the bone was fixed in 4% paraformaldehyde for further analyses.

Mouse TBI and femoral fracture model

5 of the 30 mice that randomly underwent femoral bone fractures were selected for concomitant craniocerebral injury modeling. The brain trauma model was established using the drop weight method.[59] Briefly, the mice were placed in a prone position after anesthesia, and the skull was fixed on the platform. The skull was prepared by removing hair from the surgical area and disinfected along the median line of the scalp. A 1.8 cm surgical incision was made, and a miniature skull electric drill was used to make a bone flap with a diameter of 1.5 cm at a distance of 0.5 cm from the median suture of the skull. The bone flap was removed to expose the brain tissue and a force of 4 Newtons was applied through a drop from a vertical height of 5 cm. The surgical area was disinfected, and the wound closed layer by layer. The animals were then placed in cages (1 mouse per cage) and kept warm with a warming lamp until fully awakened. Mice were then kept in a standard 12-h light and dark environment. The environment of the mice, model, such as diet, was kept consistent.

mCT analysis

mCT analysis was performed as previously described. Femurs were scanned with Bruker SkyScan 1176 mCT (2,400 frames, 5 frames/frame, 37 kV, 121 mA). The Bruker mCT analysis software (CT analysis, 3D model, CT Vol) was used to select the scan data for 3D reconstruction and bone-formation parameter analysis (Bruker, Germany). After CT scanning of the fracture model, the callus of the fracture site was harvested for H&E staining, western blotting, and RT-PCR analysis. Bone-formation parameters analyzed were: BV/TV per tissue

Table 1. Clinical information of the patients included in the study

Patients	Gender	Age (year)	Cause of injury	Fracture (Y/N)	Fracture position	TBI (Y/N)	GCS score	Time from injury to operation (day)	Fracture healing time
1	F	26	TA	N	RF	N	15	3	12
2	F	33	HP	N	LH	N	15	4	12
3	F	35	IF	N	RF	N	15	5	11
4	F	29	HP	N	RT	N	15	2	13
5	F	39	TA	N	RF	N	15	1	12
6	F	34	HP	N	LF	N	15	4	10
7	F	29	IF	N	LT	N	15	7	11
8	F	33	IF	N	LF	N	15	5	13
9	F	35	TA	N	LT	N	15	1	9
10	F	36	TA	N	LH	N	15	10	11
11	F	32	HP	Y	RF	N	15	3	13
12	F	35	HP	Y	RT	N	15	2	14
13	F	28	TA	Y	LF	N	15	4	12
14	F	32	TA	Y	RT	N	15	4	15
15	F	35	TA	Y	RF	N	15	3	14
16	F	36	IF	Y	LH	N	15	10	12
17	F	28	HP	Y	RT	N	15	5	12
18	F	28	HP	Y	RT	N	15	4	14
19	F	37	TA	Y	LH	N	15	6	12
20	F	35	TA	Y	LH	N	15	2	10
21	F	29	TA	Y	LT	Y	12	5	9
22	F	36	TA	Y	LF	Y	11	3	11
23	F	34	TA	Y	LT	Y	11	14	10
24	F	28	IF	Y	LH	Y	9	22	11
25	F	37	IF	Y	RT	Y	10	11	10
26	F	32	TA	Y	LT	Y	12	5	11
27	F	36	IF	Y	RF	Y	13	7	12
28	F	32	TA	Y	RF	Y	14	9	10
29	F	36	HP	Y	LT	Y	10	3	11
30	F	33	TA	Y	RF	Y	11	8	9

F, female; Y, yes; N, no; TBI, traumatic brain injury; GCS, Glasgow coma scale; TA, traffic accidents; HP, heavy pound; IF, injury by falling; RF, right femur; LH, left humerus; RT, right tibiae; LF, left femur; LT, left tibiae.

volume, BMD, Tb.N, cortical area fraction (Ct.Ar/Tt.Ar), average cortical thickness (Ct.Th), cortical bone area (Ct.Ar), Tb.Sp., Tb.Th, and total cross-sectional area (Tt.Ar).

Western blot analysis

Western blotting was performed as previously described.[60] Glyceraldehyde-3-phosphate dehydrogenase (GAPDH) was used for normalization. The following antibodies were used: anti-ALP (Bio-Techne, #AF2910, #MAB1448, 1:1,000), ant-Col1a1(Bio-Techne, #AF6220-SP, 1:1,000), anti-Runx2 (Bio-Techne, #AF2006-SP, 1:1,000), anti-Osteocalcin (Abcam, ab13420, 1:1,000), anti-GAPDH (Affinity, AF7021, 1:1,000), anti-P13K (Affinity, AF6241, 1:1,000), anti-Phospho-PI3K (Affinity, AF3242, 1:1,000), anti-AKT (Affinity, AF6241, 1:1,000), anti-p-AKT conjugated secondary antibodies (CST, 4060, 1:1,000), anti-AKT (CST, 9272, 1:2,000), ant-IBSP (Bio-Techne, #AF4014-SP, 1:2,000). Horseradish peroxidase (HRP)-CST were used, and protein bands were visualized and detected by using a ChemiDoc-It 610 Imaging System (UVP, Upland, CA, USA). All experiments were conducted in triplicate.

RT-PCR

TRIzol reagent (Invitrogen) was used to extract total RNA from cultured cells. RNAlater (76104; QIAGEN, Germany) was used to preserve callus samples prior to miRNA extraction, reverse

Table 2. mRNA and miRNAs primer sequences

miRNA or gene name	Primer sequence (5′ to 3′)
mmu-miRNA-92a-3p-forward	5′-TTCACTTGTCCCGGCCTGT-3′
mmu-miRNA-92a-3p- reverse	5′-CTCAACTGGTGTCGTGGAGTC-3′
hsa-miRNA-92a-3p-forward	5′-TTCACTTGTCCCGGCCTGT-3′
hsa-miRNA-92a-3p- reverse	5′-CTCAACTGGTGTCGTGGAGTC-3′
mmu-miR-U6-forward	5′-CTCGCTTCGGCAGCACAT-3′
mmu-miR-U6-reverse	5′-AACGCTTCACGAATTTGCGT-3′
hsa-IBSP-forward	5′-GAACCTCGTGGGGACAATTAC-3′
hsa-IBSP-reverse	5′-CATCATAGCCATCGTAGCCTTG-3′
mmu-IBSP-forward	5′-ACCTCGCCACCGATCAGAA-3′
mmu-IBSP-reverse	5′-TGTTGTATTCGTTGCCTGTTTGT-3′
hsa-ALP-forward	5′-ACTGGGGCCTGAGATACCC-3′
hsa-ALP-reverse	5′-TCGTGTTGCACTGGTTAAAGC-3′
mmu-ALP -forward	5′-GGCAAAGAGGGAGCTAGAA-3′
mmu-ALP-reverse	5′-ATGGCCGTGCAGATGTA-3′
hsa-COL1A1-forward	5′-GAGGGCCAAGACGAAGACATC-3′
hsa-COL1A1-reverse	5′-CAGATCACGTCATCGCACAAC-3′
mmu-COL1A1 -forward	5′-CAGAGGCGAAGGCAACA-3′
mmu-COL1A1-reverse	5′-GTCCAAGGGAGCCACATC-3′
hsa-OCN-forward	5′-GGCGCTACCTGTATCAATGG-3′
hsa-OCN-reverse	5′-GTGGTCAGCCAACTCGTCA-3′
mmu-OCN -forward	5′-GCTGTTTGTTCGGGTCTC-3′
mmu-OCN-reverse	5′-GGGCCAAAGTCAGCATC-3′
hsa-RUNX2-forward	5′-TGGTTACTGTCATGGCGGGTA-3′
hsa-RUNX2-reverse	5′-TCTCAGATCGTTGAACCTTGCTA-3′
mmu-RUNX2 -forward	5′-GCCGGGAATGATGAGAAC-3′
mmu-RUNX2-reverse	5′-TGGGGAGGATTTGTGAAGA-3′
mmu-GAPDH-forward	5′-AGGTCGGTGTGAACGGATTTG-3′
mmu-GAPDH-reverse	5′-GGGGTCGTTGATGGCAACA-3′
hsa-GAPDH-forward	5′-GGAGCGAGATCCCTCCAAAAT-3′
hsa-GAPDH-reverse	5′-GGCTGTTGTCATACTTCTCATGG-3′

transcription, and RT-PCR, which were performed according to the manufacturer's instructions. The primers used for qRT-PCR are shown in Table 2. GAPDH was used for normalization, and experiments were performed in triplicate.

Cell transfection and culture

The osteogenic precursor cell MC3T3-E1 subclone 14 was kindly donated by the Cell Resource Center of Shanghai Institute of Life Sciences, Chinese Academy of Sciences. The medium used was MEMα + medium (MEMα, 11900024, Gibco, USA), with added $NaHCO_3$ (1.5 g/L), inositol (43.2 mg/L), folic acid (8.82 mg/L), β-mercaptoethanol (7.8 mg/L, 90%), 10% high-quality fetal bovine serum (FBS, 10091148, Gibco, USA), and 1% penicillin-streptomycin (15140122, Gibco, USA). The incubator conditions were air at 95%, carbon dioxide at 5% and temperature at 37°C. MC3T3-E1 were passaged when the cell culture flask was filled to about 80%. Cells were inoculated in 6-well plate and when the cells were filled to 60%–70%, the transfection reagent lipo3000 (L3000015; Thermo Fisher Scientific, USA) was used to transfect the agomiRNA-92a-3p, antagomiRNA-92a-3p, agomiRNA-NC, antagomiRNA-NC, si-PI3K, si-AKT, and si-IBSP (GenePharma Shanghai). Transfection was carried out strictly in accordance with the lipo3000 instructions. Transfection efficiency was identified using RT-PCR and western blot.

Alizarin red staining and quantification

MC3T3-E1 subclone 14 was inoculated in a 12-well plate. After the cells adhered, they were replaced with osteogenic induction medium (HUXMA-90021; Cyagen, USA) and cultured for 3 weeks. The medium was changed once every 3 days. Pre-stained cells were washed three times with PBS (10010023; Thermo Fisher Scientific, USA) for 5 min each time to remove the residual culture medium, fixed with 95% alcohol at room temperature for 15 min, and washed with PBS three times for 5 min each time to remove excess alcohol. 1 mL of 0.5% alizarin red staining reagent was added to the well, stained at room temperature for 15 min, and washed with PBS 3–5 times for 5 min each time to remove excess staining solution. After drying, they were visualized under an inverted microscope (Olympus, BX53; Melville, NY, USA). For alizarin red staining (ARS) staining quantification, 500 μL/well (6-well plates) 10% (w/v) of cetylpyridinium chloride (Sigma, 1104006) was added to the samples and incubated for 10 min. Then 200 μL/well dissolved solution was used to measure absorbance at 562 nm by utilizing a microplate spectrophotometer (BioTek Instruments). The staining experiment was repeated three times, n = 10. Data are presented as mean ± SD (*$p < 0.05$; **$p < 0.01$; ***$p < 0.001$; # no significance).

ALP staining and quantification

MC3T3-E1 subclone 14 was inoculated in a 12-well plate. After the cells adhered, they were replaced with osteogenic induction medium (HUXMA-90021; Cyagen, USA) and cultured for 2 weeks. The medium was changed once every 3 days. The ALP color-development kit (C3206; Beyotime, China) was used according to the provided directions to assess ALP staining. Pre-stained cells were washed three times with PBS (10010023; Thermo Fisher Scientific, USA) to remove any residual culture medium; fixed with 95% alcohol at room temperature for 15 min, and washed with PBS 3 times to remove excess alcohol. 5-Bromo-4-Chloro-3-Indolyl Phosphate/ Nitroblue tetrazolium chloride (BCIP/NBT) staining working solution was added, ensuring that the sample was fully covered. The cells were incubated at room temperature in the dark for 12 h. The BCIP/NBT dyeing working solution was removed by washing with distilled water 1–2 times to halt the color reaction. After drying, the images were captured under a microscope (Olympus, BX53; Melville, NY, USA). To quantify the ALP staining, we dissolved stained cells in 10% (w/v) cetylpyridinium chloride (500 uL/wells, 6-cell plate) for 10 min, and the absorbance of the extracted solution (200 μL/cell, 96-cell plate) was measured at 562 nm (n = 3). The staining experiment was repeated three times. Data are presented as mean ± SD (*$p < 0.05$; **$p < 0.01$; ***$p < 0.001$; # no significance).

Luciferase reporter assay

A luciferase reporter assay was performed as previously described.[29] The mouse IBSP 3′ UTR region, which contains the miR-92a-3p binding sequence, was amplified by PCR from murine genomic DNA and subcloned into the Pgl3 vectore (E1741; Promega, USA). A QuikChange Site-Directed Mutagenesis Kit (210518; Stratagene, USA) was used to mutate this sequence. MC3T3-E1 subclone 14 cells (2.0×10^5 cells per well) were transiently transfected in 24-well plates with Lipofectamine 3000 (L3000015; Thermo Fisher Scientific, USA). Both 100 ng luciferase constructs and 10 ng pRL-TK (E2241; Promega, USA) Renilla luciferase plasmid were transfected into the cells, and a dual luciferase reporter assay system (E1910; Promega, USA) was used, according to the directions provided. A luminometer (Glomax, Promega) was used for quantification, with the firefly luciferase activity normalized to that of Renilla luciferase.

miRNA-92a-3p treatment on fracture model *in vivo*

In the fracture of mice, we performed local injections of agomiR-92a-3p (overexpression miR-92a-3p group, 20 μmol/L in 100 μL of PBS), antagomiR-92a-3p (silent miR-92a-3p group, 20 μmol/L in 100 μL of PBS), PBS (blank control group) at 30 μL/day. They were injected on the 1st day, 3rd day, and 7th day after surgery. After treatment with miRNA, the venous blood, callus, and femur of the mice were harvested on day 14 and day 21 after modeling for subsequent analysis.

Statistical analysis

Data are presented as the mean ± SD of at least three independent experiments. Statistical analyses were performed using GraphPad Prism 7.0 software (La Jolla, CA, USA). Differences between group means were evaluated using the one-way ANOVA or Student's t test one-way analysis. $p < 0.05$ shows statistical significance. *$p < 0.05$, **$p < 0.01$, ***$p < 0.001$, and NS means no significance.

SUPPLEMENTAL INFORMATION

Supplemental information can be found online at https://doi.org/10.1016/j.omtn.2021.02.008.

ACKNOWLEDGMENTS

This research was supported by grants (no. 81772345) from the National Natural Science Foundation of China, National Key Research & Development Program of China (nos. 2018YFC2001502 and 2018YFB1105705), National Health Commission of the People's Republic of China (nos. ZX-01-018 and ZX-01-C2016153), and the Health Commission of Hubei Province (no. WJ2019Z009).

AUTHOR CONTRIBUTIONS

L.H., B.M., and G.L. conceived and designed the experiments. Y.X., J.L., H.X., X.X., Z.L., B.M., G.L., C.Y., L.C., Y.H., and W.Z. performed the experiments. L.H., J.L., H.X., B.M., and G.L. analyzed the data. X.X., J.L., H.X., T.W., and Z.L. contributed reagents, materials, and analysis tools. J.L. and H.X. performed statistical analyses. L.H., B.M., and A.C.P. wrote the manuscript. All authors read and approved the manuscript.

DECLARATION OF INTERESTS

The authors declare no competing interests.

REFERENCES

1. Calandriello, B. (1964). CALLUS FORMATION IN SEVERE BRAIN INJURIES. Bull. Hosp. Jt. Dis. *25*, 170–175.
2. Arık, M., Ekinci, Y., Gürbüz, K., and Batın, S. (2019). The effects of focal brain damage on fracture healing: An experimental rat study. Eklem Hastalik. Cerrahisi *30*, 267–274.
3. Garland, D.E. (1988). Clinical observations on fractures and heterotopic ossification in the spinal cord and traumatic brain injured populations. Clin. Orthop. Relat. Res. (233), 86–101.
4. Brady, R.D., Grills, B.L., Church, J.E., Walsh, N.C., McDonald, A.C., Agoston, D.V., Sun, M., O'Brien, T.J., Shultz, S.R., and McDonald, S.J. (2016). Closed head experimental traumatic brain injury increases size and bone volume of callus in mice with concomitant tibial fracture. Sci. Rep. *6*, 34491.
5. Schindeler, A., McDonald, M.M., Bokko, P., and Little, D.G. (2008). Bone remodeling during fracture repair: The cellular picture. Semin. Cell Dev. Biol. *19*, 459–466.
6. Rauch, A., Haakonsson, A.K., Madsen, J.G.S., Larsen, M., Forss, I., Madsen, M.R., Van Hauwaert, E.L., Wiwie, C., Jespersen, N.Z., Tencerova, M., et al. (2019). Osteogenesis depends on commissioning of a network of stem cell transcription factors that act as repressors of adipogenesis. Nat. Genet. *51*, 716–727.
7. Fan, Y., Hanai, J.I., Le, P.T., Bi, R., Maridas, D., DeMambro, V., Figueroa, C.A., Kir, S., Zhou, X., Mannstadt, M., et al. (2017). Parathyroid Hormone Directs Bone Marrow Mesenchymal Cell Fate. Cell Metab. *25*, 661–672.
8. Hu, K., and Olsen, B.R. (2016). Osteoblast-derived VEGF regulates osteoblast differentiation and bone formation during bone repair. J. Clin. Invest. *126*, 509–526.
9. Liu, C.J., Chang, E., Yu, J., Carlson, C.S., Prazak, L., Yu, X.P., Ding, B., Lengyel, P., and Di Cesare, P.E. (2005). The interferon-inducible p204 protein acts as a transcriptional coactivator of Cbfa1 and enhances osteoblast differentiation. J. Biol. Chem. *280*, 2788–2796.
10. Eijken, M., Koedam, M., van Driel, M., Buurman, C.J., Pols, H.A., and van Leeuwen, J.P. (2006). The essential role of glucocorticoids for proper human osteoblast differentiation and matrix mineralization. Mol. Cell. Endocrinol. *248*, 87–93.
11. Guo, J., Qin, W., Xing, Q., Gao, M., Wei, F., Song, Z., Chen, L., Lin, Y., Gao, X., and Lin, Z. (2017). TRIM33 is essential for osteoblast proliferation and differentiation via BMP pathway. J. Cell. Physiol. *232*, 3158–3169.
12. Kim, V.N., Han, J., and Siomi, M.C. (2009). Biogenesis of small RNAs in animals. Nat. Rev. Mol. Cell Biol. *10*, 126–139.
13. Bartel, D.P. (2004). MicroRNAs: genomics, biogenesis, mechanism, and function. Cell *116*, 281–297.
14. Lian, J.B., Stein, G.S., van Wijnen, A.J., Stein, J.L., Hassan, M.Q., Gaur, T., and Zhang, Y. (2012). MicroRNA control of bone formation and homeostasis. Nat. Rev. Endocrinol. *8*, 212–227.
15. Li, C.J., Cheng, P., Liang, M.K., Chen, Y.S., Lu, Q., Wang, J.Y., Xia, Z.Y., Zhou, H.D., Cao, X., Xie, H., et al. (2015). MicroRNA-188 regulates age-related switch between osteoblast and adipocyte differentiation. J. Clin. Invest. *125*, 1509–1522.
16. Wang, R., Zhang, H., Ding, W., Fan, Z., Ji, B., Ding, C., Ji, F., and Tang, H. (2020). miR-143 promotes angiogenesis and osteoblast differentiation by targeting HDAC7. Cell Death Dis. *11*, 179.
17. Redell, J.B., Liu, Y., and Dash, P.K. (2009). Traumatic brain injury alters expression of hippocampal microRNAs: potential regulators of multiple pathophysiological processes. J. Neurosci. Res. *87*, 1435–1448.
18. Redell, J.B., Moore, A.N., Ward, N.H., 3rd, Hergenroeder, G.W., and Dash, P.K. (2010). Human traumatic brain injury alters plasma microRNA levels. J. Neurotrauma *27*, 2147–2156.
19. Mao, G., Zhang, Z., Hu, S., Zhang, Z., Chang, Z., Huang, Z., Liao, W., and Kang, Y. (2018). Exosomes derived from miR-92a-3p-overexpressing human mesenchymal stem cells enhance chondrogenesis and suppress cartilage degradation via targeting WNT5A. Stem Cell Res. Ther. *9*, 247.
20. He, S., Wang, Z., Li, Y., Dong, J., Xiang, D., Ren, L., Guo, L., and Shu, J. (2020). MicroRNA-92a-3p enhances functional recovery and suppresses apoptosis after spinal cord injury via targeting phosphatase and tensin homolog. Biosci. Rep. *40*, BSR20192743.

21. Kerr, J.M., Fisher, L.W., Termine, J.D., Wang, M.G., McBride, O.W., and Young, M.F. (1993). The human bone sialoprotein gene (IBSP): genomic localization and characterization. Genomics *17*, 408–415.

22. Wang, J., Wang, L., Xia, B., Yang, C., Lai, H., and Chen, X. (2013). BSP gene silencing inhibits migration, invasion, and bone metastasis of MDA-MB-231BO human breast cancer cells. PLoS ONE *8*, e62936.

23. Ayari, H., and Bricca, G. (2012). Microarray analysis reveals overexpression of IBSP in human carotid plaques. Adv. Med. Sci. *57*, 334–340.

24. Curtin, P., McHugh, K.P., Zhou, H.Y., Flückiger, R., Goldhaber, P., Oppenheim, F.G., and Salih, E. (2009). Modulation of bone resorption by phosphorylation state of bone sialoprotein. Biochemistry *48*, 6876–6886.

25. Guntur, A.R., and Rosen, C.J. (2011). The skeleton: a multi-functional complex organ: new insights into osteoblasts and their role in bone formation: the central role of PI3Kinase. J. Endocrinol. *211*, 123–130.

26. Marie, P.J. (2012). Signaling pathways affecting skeletal health. Curr. Osteoporos. Rep. *10*, 190–198.

27. Cadosch, D., Gautschi, O.P., Thyer, M., Song, S., Skirving, A.P., Filgueira, L., and Zellweger, R. (2009). Humoral factors enhance fracture-healing and callus formation in patients with traumatic brain injury. J. Bone Joint Surg. Am. *91*, 282–288.

28. Lin, Z., Tang, Y., Tan, H., and Cai, D. (2019). MicroRNA-92a-1-5p influences osteogenic differentiation of MC3T3-E1 cells by regulating β-catenin. J. Bone Miner. Metab. *37*, 264–272.

29. Xiong, Y., Cao, F., Hu, L., Yan, C., Chen, L., Panayi, A.C., Sun, Y., Zhou, W., Zhang, P., Wu, Q., et al. (2019). miRNA-26a-5p Accelerates Healing via Downregulation of PTEN in Fracture Patients with Traumatic Brain Injury. Mol. Ther. Nucleic Acids *17*, 223–234.

30. Wang, L., Yu, C., Zhang, Y., Luo, L., and Zhang, G. (2018). An analysis of the characteristics of road traffic injuries and a prediction of fatalities in China from 1996 to 2015. Traffic Inj. Prev. *19*, 749–754.

31. Adeloye, D., Thompson, J.Y., Akanbi, M.A., Azuh, D., Samuel, V., Omoregbe, N., and Ayo, C.K. (2016). The burden of road traffic crashes, injuries and deaths in Africa: a systematic review and meta-analysis. Bull. World Health Organ. *94*, 510–521A.

32. Nepal, S., Gupta, S., Wong, E.G., Gurung, S., Swaroop, M., Kushner, A.L., and Nwomeh, B.C. (2015). Burden of road traffic injuries in Nepal: results of a country-wide population-based survey. Lancet *385* (*Suppl 2*), S7.

33. Maiden, M.J., Cameron, P.A., Rosenfeld, J.V., Cooper, D.J., McLellan, S., and Gabbe, B.J. (2020). Long-Term Outcomes after Severe Traumatic Brain Injury in Older Adults. A Registry-based Cohort Study. Am. J. Respir. Crit. Care Med. *201*, 167–177.

34. Golinvaux, N.S., Labrum, J.T., Lee, D.H., and Desai, M.J. (2020). Symptomatic Radial Neck Nonunion Following Traumatic Impacted Radial Neck Fracture. J. Hand Surg. Am. *45*, 453.e1–453.e5.

35. Lu, S., Du, T., Sun, Z., Xu, L., Tong, X., and Yan, H. (2020). Timing of Extremity Fracture Fixation in Patients with Traumatic Brain Injury: A Meta-Analysis of Prognosis. World Neurosurg. *133*, 227–236.

36. Luo, H., Su, Y., Ding, L., Xiao, H., Wu, M., and Xue, F. (2019). Exchange nailing versus augmentative plating in the treatment of femoral shaft nonunion after intramedullary nailing: a meta-analysis. EFORT Open Rev. *4*, 513–518.

37. Zhang, W., Zhang, Z., and Chen, H. (2019). [Research progress of augmentation plate for femoral shaft nonunion after intramedullary nail fixation]. Zhongguo Xiu Fu Chong Jian Wai Ke Za Zhi *33*, 1467–1473.

38. Locher, R.J., Lünnemann, T., Garbe, A., Schaser, K., Schmidt-Bleek, K., Duda, G., and Tsitsilonis, S. (2015). Traumatic brain injury and bone healing: radiographic and biomechanical analyses of bone formation and stability in a combined murine trauma model. J. Musculoskelet. Neuronal Interact. *15*, 309–315.

39. Yang, T.Y., Wang, T.C., Tsai, Y.H., and Huang, K.C. (2012). The effects of an injury to the brain on bone healing and callus formation in young adults with fractures of the femoral shaft. J. Bone Joint Surg. Br. *94*, 227–230.

40. Polito, F., Famà, F., Oteri, R., Raffa, G., Vita, G., Conti, A., Daniele, S., Macaione, V., Passalacqua, M., Cardali, S., et al. (2020). Circulating miRNAs expression as potential biomarkers of mild traumatic brain injury. Mol. Biol. Rep. *47*, 2941–2949.

41. Treiber, T., Treiber, N., and Meister, G. (2019). Regulation of microRNA biogenesis and its crosstalk with other cellular pathways. Nat. Rev. Mol. Cell Biol. *20*, 5–20.

42. Huang, X., Xiong, X., Liu, J., Zhao, Z., and Cen, X. (2020). MicroRNAs-containing extracellular vesicles in bone remodeling: An emerging frontier. Life Sci. *254*, 117809.

43. Edwards, K.A., Pattinson, C.L., Guedes, V.A., Peyer, J., Moore, C., Davis, T., Devoto, C., Turtzo, L.C., Latour, L., and Gill, J.M. (2020). Inflammatory Cytokines Associate With Neuroimaging After Acute Mild Traumatic Brain Injury. Front. Neurol. *11*, 348.

44. Seemann, R., Graef, F., Garbe, A., Keller, J., Huang, F., Duda, G., Schmidt-Bleek, K., Schaser, K.D., and Tsitsilonis, S. (2018). Leptin-deficiency eradicates the positive effect of traumatic brain injury on bone healing: histological analyses in a combined trauma mouse model. J. Musculoskelet. Neuronal Interact. *18*, 32–41.

45. Singleton, Q., Vaibhav, K., Braun, M., Patel, C., Khayrullin, A., Mendhe, B., Lee, B.R., Kolhe, R., Kaiser, H., Awad, M.E., et al. (2019). Bone Marrow Derived Extracellular Vesicles Activate Osteoclast Differentiation in Traumatic Brain Injury Induced Bone Loss. Cells *8*, 63.

46. Lee, S.Y., Yang, J., Park, J.H., Shin, H.K., Kim, W.J., Kim, S.Y., Lee, E.J., Hwang, I., Lee, C.S., Lee, J., and Kim, H.S. (2020). The MicroRNA-92a/Sp1/MyoD Axis Regulates Hypoxic Stimulation of Myogenic Lineage Differentiation in Mouse Embryonic Stem Cells. Mol. Ther. *28*, 142–156.

47. de Miguel Pérez, D., Rodriguez Martínez, A., Ortigosa Palomo, A., Delgado Ureña, M., Garcia Puche, J.L., Robles Remacho, A., Exposito Hernandez, J., Lorente Acosta, J.A., Ortega Sánchez, F.G., and Serrano, M.J. (2020). Extracellular vesicle-miRNAs as liquid biopsy biomarkers for disease identification and prognosis in metastatic colorectal cancer patients. Sci. Rep. *10*, 3974.

48. Bouleftour, W., Boudiffa, M., Wade-Gueye, N.M., Bouët, G., Cardelli, M., Laroche, N., Vanden-Bossche, A., Thomas, M., Bonnelye, E., Aubin, J.E., et al. (2014). Skeletal development of mice lacking bone sialoprotein (BSP)–impairment of long bone growth and progressive establishment of high trabecular bone mass. PLoS ONE *9*, e95144.

49. Boudiffa, M., Wade-Gueye, N.M., Guignandon, A., Vanden-Bossche, A., Sabido, O., Aubin, J.E., Jurdic, P., Vico, L., Lafage-Proust, M.H., and Malaval, L. (2010). Bone sialoprotein deficiency impairs osteoclastogenesis and mineral resorption in vitro. J. Bone Miner. Res. *25*, 2669–2679.

50. LoRusso, P.M. (2016). Inhibition of the PI3K/AKT/mTOR Pathway in Solid Tumors. J. Clin. Oncol. *34*, 3803–3815.

51. Iffland, P.H., 2nd, and Crino, P.B. (2017). Focal Cortical Dysplasia: Gene Mutations, Cell Signaling, and Therapeutic Implications. Annu. Rev. Pathol. *12*, 547–571.

52. Yang, A., Lu, Y., Xing, J., Li, Z., Yin, X., Dou, C., Dong, S., Luo, F., Xie, Z., Hou, T., and Xu, J. (2018). IL-8 Enhances Therapeutic Effects of BMSCs on Bone Regeneration via CXCR2-Mediated PI3k/Akt Signaling Pathway. Cell. Physiol. Biochem. *48*, 361–370.

53. Han, Y., Wang, X., Ma, D., Wu, X., Yang, P., and Zhang, J. (2018). Ipriflavone promotes proliferation and osteogenic differentiation of periodontal ligament cells by activating GPR30/PI3K/AKT signaling pathway. Drug Des. Devel. Ther. *12*, 137–148.

54. Liu, Y., Wang, H., Zhou, X.Z., Li, N., Guo, Y.C., and Chen, T.P. (2020). Pentraxin 3 promotes the osteoblastic differentiation of MC3T3-E1 cells through the PI3K/Akt signaling pathway. Biosci. Rep. *40*, BSR20201165.

55. Deng, S., Dai, G., Chen, S., Nie, Z., Zhou, J., Fang, H., and Peng, H. (2019). Dexamethasone induces osteoblast apoptosis through ROS-PI3K/AKT/GSK3β signaling pathway. Biomed. Pharmacother. *110*, 602–608.

56. Perkins, R., and Skirving, A.P. (1987). Callus formation and the rate of healing of femoral fractures in patients with head injuries. J. Bone Joint Surg. Br. *69*, 521–524.

57. Teasdale, G., Maas, A., Lecky, F., Manley, G., Stocchetti, N., and Murray, G. (2014). The Glasgow Coma Scale at 40 years: standing the test of time. Lancet Neurol. *13*, 844–854.

58. Luo, Z.W., Li, F.X., Liu, Y.W., Rao, S.S., Yin, H., Huang, J., Chen, C.Y., Hu, Y., Zhang, Y., Tan, Y.J., et al. (2019). Aptamer-functionalized exosomes from bone marrow stromal cells target bone to promote bone regeneration. Nanoscale *11*, 20884–20892.

59. Flierl, M.A., Stahel, P.F., Beauchamp, K.M., Morgan, S.J., Smith, W.R., and Shohami, E. (2009). Mouse closed head injury model induced by a weight-drop device. Nat. Protoc. *4*, 1328–1337.

60. Xue, H., Hu, L., Xiong, Y., Zhu, X., Wei, C., Cao, F., Zhou, W., Sun, Y., Endo, Y., Liu, M., et al. (2019). Quaternized chitosan-Matrigel-polyacrylamide hydrogels as wound dressing for wound repair and regeneration. Carbohydr. Polym. *226*, 115302.

OMTN, Volume *23*

Supplemental information

miRNA-92a-3p regulates osteoblast differentiation in patients with concomitant limb fractures and TBI via IBSP/PI3K-AKT inhibition

Liangcong Hu, Jing Liu, Hang Xue, Adriana C. Panayi, Xudong Xie, Ze Lin, Tiantian Wang, Yuan Xiong, Yiqiang Hu, Chengcheng Yan, Lang Chen, Abudula Abududilibaier, Wu Zhou, Bobin Mi, and Guohui Liu

Figure S1. Quantitative comparison of fracture healing time in clinical patients

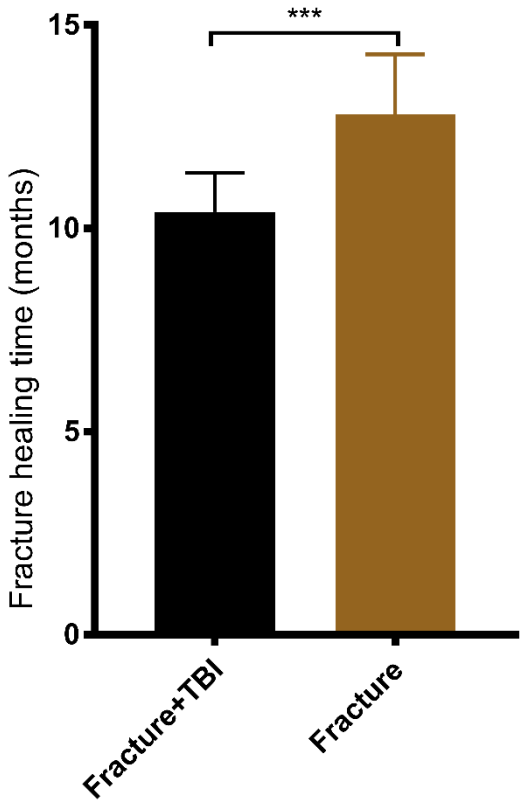

Quantitative analysis and comparison of fracture healing time in patients with concomitant limb fractures and traumatic brain injury and patients with simple fracture. N=10, Data are presented as mean±SD (*p<0.05; **p<0.01; ***p<0.001; # no significance).

Figure S2. Group quantitative analysis of local fracture callus volume in clinical patients

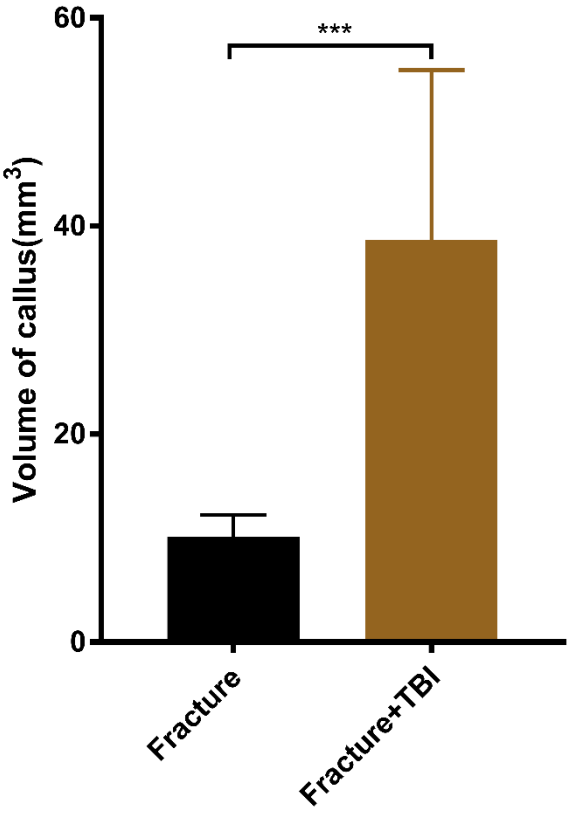

Refer to the Per-kins callus volume calculation method. In short, the formula is V=2*Π*r1*(r2-r1) * l; r1=radius of bone; r2=radius of bone plus callus; l= length of callus. The last front and lateral X-rays of the limbs before the operation are used to calculate the callus volume. N=10, Data are presented as mean±SD (*p<0.05; **p<0.01; ***p<0.001; # no significance).

Figure S3. Quantitative analysis of relative ALP activity

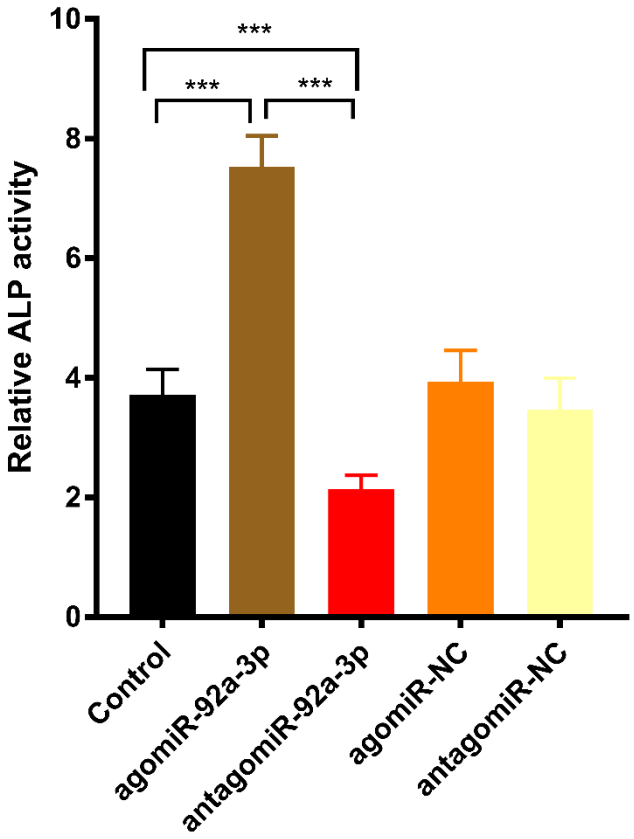

In order to quantify the relative ALP activity, the stained cells were dissolved in 10% (w/v) cetylpyridinium chloride for 10 minutes and extracted by absorbance measurement at 562 nm the solution. Quantitative analysis of relative ALP activity in Figure 3G, N=3, Data are presented as mean±SD (*p<0.05; **p<0.01; ***p<0.001; # no significance).

Figure S4. Calcium deposition detection by Alizarin Red staining

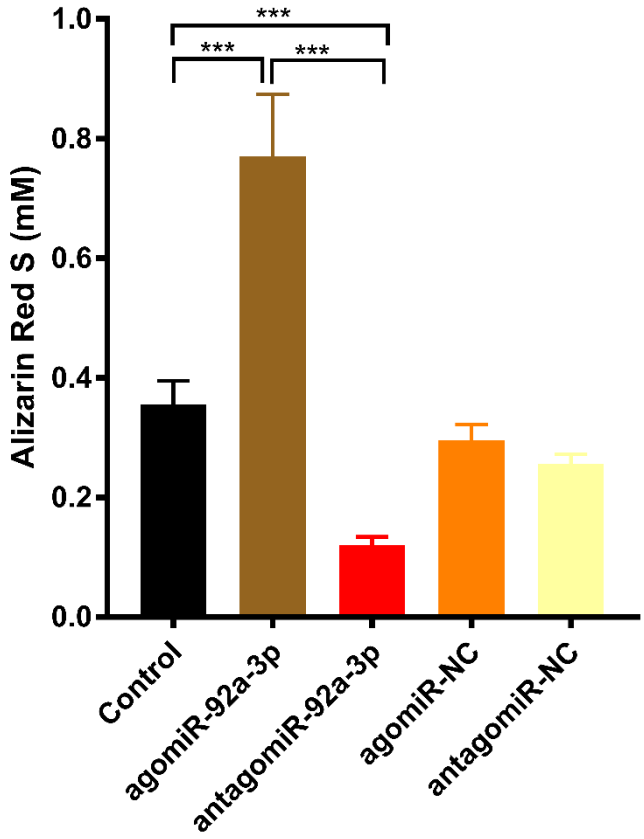

Alizarin red-S staining was quantified by densitometry at 562 nm. Quantitative analysis of Alizarin Red staining in Figure 3H, N=3, Data are presented as mean±SD (*p<0.05; **p<0.01; ***p<0.001; # no significance).

Figure S5. Quantitative analysis of relative ALP activity

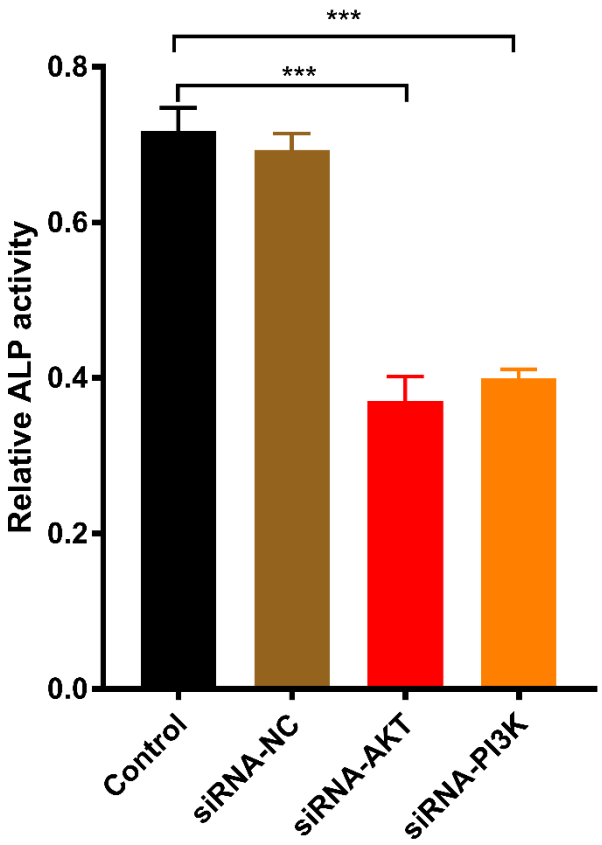

In order to quantify the relative ALP activity, the stained cells were dissolved in 10% (w/v) cetylpyridinium chloride for 10 minutes and extracted by absorbance measurement at 562 nm the solution. Quantitative analysis of relative ALP activity in Figure 5J, N=3, Data are presented as mean±SD (*p<0.05; **p<0.01; ***p<0.001; # no significance).

Figure S6. Calcium deposition detection by Alizarin Red staining

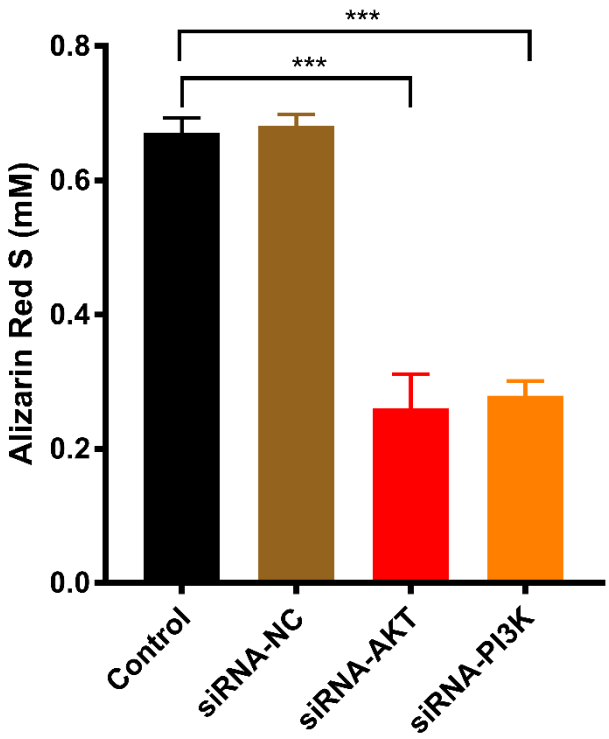

Alizarin red-S staining was quantified by densitometry at 562 nm. Quantitative analysis of Alizarin Red staining in Figure 5I, N=3, Data are presented as mean±SD (*p<0.05; **p<0.01; ***p<0.001; # no significance).